# Architecture of optical fiber sensor for the simultaneous measurement of axial and radial strains

Dominique Leduc, Yann Lecieux, Pierre-Antoine Morvan, Cyril Lupi

# Architecture of optical fiber sensor for the simultaneous measurement of axial and radial strains

**Dominique Leduc, Yann Lecieux, Pierre-Antoine Morvan and Cyril Lupi**

L'UNAM Université, Université de Nantes, UFR Sciences et Techniques, Institut de Recherche en Génie Civil et Mécanique, GeM—UMR CNRS 6183, 2 rue de la Houssinière, F-44322 Nantes, France

E-mail: dominique.leduc@univ-nantes.fr

**Abstract**
The aim of this paper is to investigate the ability to measure simultaneously the axial and radial strain with a single optical fiber sensor. The discussion begins with the analytical study of a cylinder subjected to pure tensile strain and thermal load. We emphasize the necessity of measuring the radial strain in order to determine the axial strain of an embedded sensor with accuracy. Then, we describe a few sensors able to measure axial and radial strains and study their efficiency. The conclusion is that the best structure is made of the juxtaposition of a short and a long period grating.

## 1. Introduction

Fiber Bragg gratings (FBGs) are written in optical fibers by UV irradiation. An interferometric device creates fringes inside the core of the fiber. The periodic variation of the UV light intensity in the longitudinal direction induces a periodic variation of the refractive index of the core. As a consequence, the grating behaves like an interferential filter. It reflects a very narrow spectral band of the incoming light, centered on the Bragg wavelength:

$$\lambda_B = 2n_{\text{eff}}\Lambda_0 \qquad (1)$$

where $n_{\text{eff}}$ is the effective index of the mode that propagates inside the core and $\Lambda_0$ is the period of modulation. This behavior is a very interesting feature for sensing applications. Indeed, any external constraint that modifies the effective index or the period of modulation induces a shift in the Bragg wavelength:

$$\frac{\Delta\lambda_B}{\lambda_B} = \frac{\Delta n_{\text{eff}}}{n_{\text{eff}}} + \frac{\Delta\Lambda_0}{\Lambda_0}. \qquad (2)$$

The measurement of this shift can lead to the applied load if the sensor has been previously calibrated or if an appropriate model is available. This measure is robust since it is wavelength encoded and does not depend on intensity fluctuations.

FBG strain sensors are nowadays commercially available, but these commercial sensors are restricted to the measurement of axial strain. They have to be placed on the surface of the monitored structure, glued on two points and free to undergo deformation in the transverse plane. Under these conditions they give reliable results with an accuracy of approximately 1 $\mu\epsilon$, but they may give erroneous results when embedded in a material. Indeed, in order to analyze the Bragg wavelength shift, a restrictive assumption is classically made to link the axial and radial strains. In section 2, we study the limits of this assumption and present some situations where it does not hold. In such cases, both axial and radial strain have to be measured in order to reliably determine the axial strain.

The determination of both strains requires two independent measurements. At first glance, the easiest solution is to use two different sensors, for example two FBGs. However, this can work only if the two sensors measure different components of the same strain tensor. In real structures with complex geometry and load, a strain gradient between both sensors is very likely, which limits the practical interest of this solution.

The best solution would be to design a compact sensor, included in a single fiber, interrogated by classical means. A

good starting point is given by all the works performed on the simultaneous measurements of strain and temperature with optical fiber sensors. Several architectures are available: an FBG coupled with a Fabry–Perot cavity [1, 2], an FBG written in a birefringent fiber, two superimposed FBGs with different periods [3], and an FBG juxtaposed with a long period grating (LPG) [4, 5]. We shall focus on the last three structures since the first one lacks compactness. These structures are presented and their efficiency studied in section 3. From this study, we recommend in section 4 the use of the architecture with an FBG and an LPG.

## 2. Why measure simultaneously the strains $\varepsilon_z$ and $\varepsilon_r$ of an FBG to perform the analysis of mechanical loads?

The FBGs have been employed for many years in the field of strain measurement. They are widely used in devices such as strain gauge rosettes stuck on the surface of the studied object. The analysis of data obtained with such surface sensors is well known and provides reliable information on the strain of the studied structure following the direction of the sensor axis (see [6]).

Because of their small size, the fiber-optic sensors are now embedded in mechanical components, such as resin parts (polyester or epoxy) to perform structural health monitoring or production process monitoring [2, 7, 8].

We are interested in this field of applications. When a sensor is embedded, the observation of only one shift in Bragg wavelength is not enough to accurately measure its axial strain. To explain it, we have to discuss the hypotheses needed to obtain the commonly used relations giving the shift in Bragg wavelength $\frac{\Delta\lambda_B}{\lambda_B}$ as a function of the FBG axial strain $\varepsilon_{33} = \varepsilon_z$. This discussion is given in section 2.1. Next in sections 2.2 and 2.3 we give some examples of the error incurred in the measurement of an FBG axial strain when its radial strain is unknown (i.e. when a specific measure allowing us to know the FBG radial strain has not been obtained).

### 2.1. Classical theory of the strain measurement using an FBG

When a material is subjected to an external load, it becomes deformed along several directions. The strains induce refractive index change due to the photo-elastic effect:

$$\Delta\left(\frac{1}{n_{ij}^2}\right) = p_{ijkl}\varepsilon_{kl} \qquad (i, j, k, l = 1, 2, 3) \qquad (3)$$

where $p_{ijkl}$ are the components of the photo-elastic tensor. For a classic optical fiber, when the strain is isotropic in the cross section of the sensor, the effective index change is only written as

$$\frac{\Delta n_{\text{eff}}}{n_{\text{eff}}} = -\frac{n_{\text{eff}}^2}{2}\left[(p_{11} + p_{12})\varepsilon_r + p_{12}\varepsilon_z\right] \qquad (4)$$

where $\varepsilon_r = \varepsilon_{11} = \varepsilon_{22}$ is the radial strain and $\varepsilon_z = \varepsilon_{33}$ the axial strain [9]. The strain variation leads to a shift in Bragg
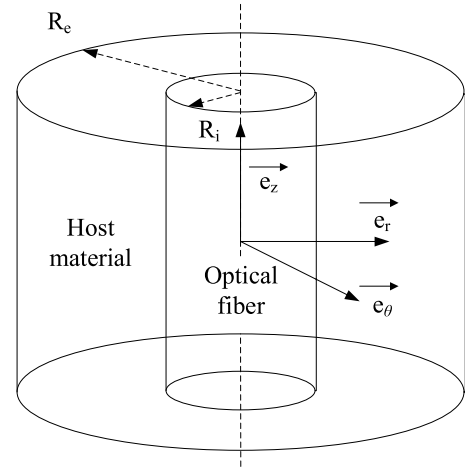


**Figure 1.** Specimen instrumented with an FBG: geometry.

wavelength. According to (2), it is given by

$$\frac{\Delta\lambda_B}{\lambda_B} = -\frac{n_{\text{eff}}^2}{2}(p_{11} + p_{12})\varepsilon_r + \left(1 - \frac{n_{\text{eff}}^2}{2}p_{12}\right)\varepsilon_z. \qquad (5)$$

As we can see, the shift in Bragg wavelength is a function of two unknown physical quantities. Now, if we consider the case where the optical fiber is only glued at two points on the studied structure, the axial sensor strain is exactly equal to the strain of the structure along the direction of the sensor axis. Moreover, the optical fiber is free to become deformed along its radial direction. The fiber radial strain is then the product of the sensor axial strain by the Poisson ratio: $\varepsilon_r = -\nu\varepsilon_z$. In such a case, only one quantity is unknown: $\varepsilon_z$. It can be found by measuring only one shift in Bragg wavelength:

$$\frac{\Delta\lambda_B}{\lambda_B} = \left\{1 - \frac{n_{\text{eff}}^2}{2}\left[p_{12} - \nu(p_{11} + p_{12})\right]\right\}\varepsilon_z. \qquad (6)$$

Equation (6) is widely used in the scientific literature and often presented as a universal relation between the FBG axial strain and the shift in Bragg wavelength. In reality, it can be used only in the specific conditions that we have previously explained. When misused, relation (6) leads to incorrect results. To show this, we study a cylindrical sample subjected to mechanical and thermal loads.

### 2.2. Study of a cylinder in uniaxial tension

Consider an FBG embedded in the center of a cylindrical specimen of radius $R_e$ made of homogeneous and isotropic material (see figure 1). A uniform tensile strain is imposed on the specimen $\varepsilon_z \approx \sigma_z^h/E^h$ but it stays free to undergo deformation in the radial direction. The model chosen to represent the optical fiber is a homogeneous and isotropic cylinder of silica. The elastic constants of the fiber are $E^f$ and $\nu^f$ while the elastic constants of the host material are $E^h$ and $\nu^h$.

The study of a cylindrical specimen in uniaxial tension is a classical problem (see [10]). The displacement field for one

cylinder is written as

$$\overrightarrow{u} = \begin{cases} u_r \overrightarrow{e_r} \\ u_z \overrightarrow{e_z} \end{cases} = \begin{cases} Cr + \dfrac{D}{r} \overrightarrow{e_r} \\ Kz \overrightarrow{e_z} \end{cases} \tag{7}$$

where $C$, $D$ and $K$ are constants given by the boundary conditions, and $r$ the current radial coordinate in the cylinder. By using this displacement field, we obtain the strain tensor $\overline{\overline{\varepsilon}}$ as $\overline{\overline{\varepsilon}} = \frac{1}{2}(\nabla \overrightarrow{u} + \nabla \overrightarrow{u}^T)$, which gives

$$\overline{\overline{\varepsilon}} = \begin{bmatrix} C - \dfrac{D}{r^2} & & \\ & C + \dfrac{D}{r^2} & \\ & & K \end{bmatrix}. \tag{8}$$

Then, using Hooke's law, we obtain the stress tensor: $\overline{\overline{\sigma}} = \lambda tr(\overline{\overline{\varepsilon}})\overline{\overline{I}} + 2\mu\overline{\overline{\varepsilon}}$ with $\mu = \frac{E}{2(1+\nu)}$ and $\lambda = \frac{\nu E}{(1-2\nu)(1+\nu)}$. In this document, the quantities with superscript f refer to the FBG, while those with superscript h refer to the host material.

We also call respectively $\overrightarrow{u}^{\,f}$, $\overline{\overline{\sigma^f}}$ and $\overline{\overline{\varepsilon^f}}$ the displacement field, the stress and strain tensor of the optical fiber while the notations $\overrightarrow{u}^{\,h}$, $\overline{\overline{\sigma^h}}$ and $\overline{\overline{\varepsilon^h}}$ refer to the displacement field, the stress and strain tensor of the specimen. The strain and stress tensors are different in the fiber and in the specimen. Thus, we need to calculate six components in order to solve the mechanical problem, i.e. $C^f, D^f, K^f, C^h, D^h, K^h$. The following boundary conditions allow us to find their expressions:

- no radial displacement at $r = 0$

$$u_r^f(0) = 0 \Rightarrow D^f = 0 \tag{9}$$

- equality of the axial displacement

$$u_z^f = u_z^h \Rightarrow K^f = K^h = \varepsilon_z \approx \frac{\sigma_z^h}{E^h} \tag{10}$$

- continuity of the radial displacement at the interface between the FBG and the specimen

$$u_r^h(R_i) = u_r^f(R_i) \Rightarrow C^h R_i + \frac{D^h}{R_i} = C^f R_i \tag{11}$$

- continuity of the radial stress at the interface

$$\sigma_{rr}^f(R_i) = \sigma_{rr}^h(R_i) \Rightarrow \lambda^f(2C^f + K) + 2\mu^f C^f$$
$$= 2\mu^h \left( C^h - \frac{D^h}{R_i^2} \right) + \lambda^h(2C^h + K) \tag{12}$$

- no radial stress on the specimen external surface

$$\sigma_{rr}^h(R_e) = 0 \Rightarrow 2\mu^h \left( C^h - \frac{D^h}{R_e^2} \right) + \lambda^h(2C^h + K) = 0. \tag{13}$$

The expressions obtained for $C^f$, $C^h$ and $D^h$ are then simplified with the hypothesis of an infinite host material as compared with the radial dimension of the fiber. We also
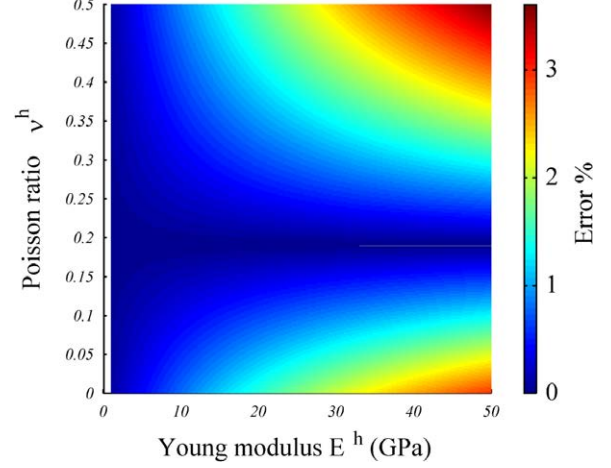


**Figure 2.** Difference between the real model (equations (5) and (14)) and the commonly used model (equation (6)) depending on the host material properties.

suppose that $\frac{R_i^2}{R_e^2} \simeq 0$. In order to calculate the stress tensor in the specimen, we consider a particle far from the FBG. This amounts to neglecting $\frac{R_i^2}{r^2}$ because $r \to R_e$. Thus, the obtained result can be used for any section of homogeneous and isotropic material in uniaxial tension.

$$D^f = 0 \qquad D^h \approx 0$$
$$\varepsilon_r^h = C^h \approx -\nu^h \varepsilon_z \tag{14}$$
$$\varepsilon_r^f = C^f \approx -\kappa \varepsilon_z$$

with

$$\kappa = \frac{-\nu^f E^f - \nu^f E^f \nu^h - \nu^h E^h + \nu^h E^h \nu^f + 2\nu^h E^h (\nu^f)^2}{-E^f - E^f \nu^h - E^h + E^h \nu^f + 2E^h (\nu^f)^2}.$$

As we can see in the previous equation, the radial strain $\varepsilon_r^f = C^f \approx -\kappa \varepsilon_z$ is really constant in the FBG but it is not equal to $-\nu^f \varepsilon_z$. There is a mechanical coupling between the strain in the specimen and in the fiber. Consequently, the strain in the fiber depends on the properties of the material in which it is embedded. Thus, using equation (6) considering $\varepsilon_r^f = -\nu \varepsilon_z$ is failing to estimate $\varepsilon_z$. The error incurred depends on the properties of the couple of the material used for the specimen and the optical fiber. Figure 2 allows us to estimate it. It shows the relative difference between $\varepsilon_z$ calculated with the approximated relation $\varepsilon_r^f = -\nu^f \varepsilon_z$ and $\varepsilon_z$ calculated with the correct relation $\varepsilon_r^f = -\kappa \varepsilon_z$ for a given $\frac{\Delta \lambda}{\lambda}$ (calculated with $p_{11} = 0.113$, $p_{12} = 0.252$, $n_{\text{eff}} = 1.447\,467$ [11]). In order to draw this figure, we have considered the following material properties for the optical fiber $\nu^f = 0.19$ and $E^f = 75\,300$ MPa.

Figure 2 shows that, even in a really simple problem, the knowledge of $\frac{\Delta \lambda}{\lambda}$ is not enough to accurately estimate the FBG axial strain and then the strain of the studied structure. To perform such measurements, several methods are possible:

- to have the knowledge of $\varepsilon_r$ and use the relation (5);
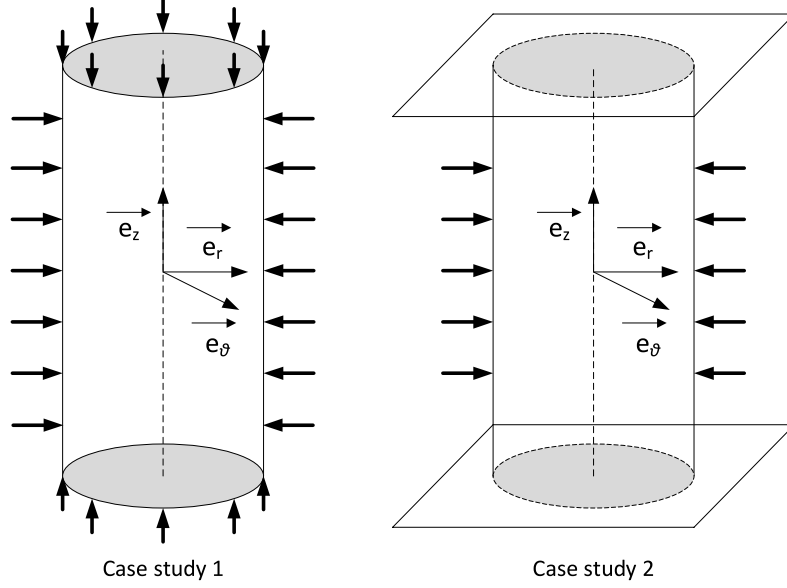- to perform an experimental calibration of the sensor [12];

**Figure 3.** The two different boundary conditions for the cylinder in thermal load analysis.

- to use the previous analytical model, which implies having a thorough knowledge of $E^h$ and $\nu^h$.

### 2.3. Study of a cylinder subjected to thermal loads

Consider now a fiber embedded in a heat hardening resin as used in the composite material. We suppose that an FBG has been set up in the mold before resin injection. The initially liquid resin is heated and becomes solid. During cooling, it imposes mechanical stress on the fiber axially as well as radially. This case should occur in production process monitoring. Thanks to the study of two academic problems, we shall explain how to analyze the shift in Bragg wavelength that we could observe in such a case.

The object of our study is an epoxy resin cylinder. In its center, an FBG is embedded. A drop of 100 K in temperature is imposed on the structure. The material properties of the sensor and the resin are given in table 1.

As in the previous problem, the displacement and strain field are given by relations (7) and (8). Nevertheless, Hooke's law includes here an additional term relative to the thermal change, i.e.

$$\overline{\overline{\sigma}} = \lambda tr(\overline{\overline{\varepsilon}})\overline{\overline{I}} + 2\mu\overline{\overline{\varepsilon}} - (3\lambda + 2\mu)\alpha\Delta T \overline{\overline{I}} \tag{15}$$

where $\alpha$ is the thermal expansion coefficient.

Two different boundary conditions are considered here (cf figure 3). First, the cylinder is free to undergo axial and radial deformations. In the second case, the radial surface is free while the upper and lower sections are fixed.

#### 2.3.1. Case study 1: the cylinder is free to undergo axial and radial deformations.
In this first thermal load, the drop in temperature leads to the negative expansion of the host cylinder axially as well as radially. For a resin structure such as $R_e \gg R_i$ we have $\varepsilon_r^h \approx \varepsilon_z^h \approx -\alpha^h \Delta T$.

**Table 1.** Geometry and material properties of resin cylinder instrumented with an FBG.

|  | FBG | Resin |
|---|---|---|
| E (MPa) | 75 300 | 3100 |
| $\nu$ | 0.19 | 0.4 |
| $\alpha$ (K$^{-1}$) | $5 \times 10^{-7}$ | $114 \times 10^{-6}$ |
| $\phi$ | 125 $\mu$m | 20 mm |

To calculate the strain field in the FBG with such boundary conditions, we can use the equations (9) and (11) related to the radial displacements. The continuity of the radial stress at the interface between the FBG and the resin $\sigma_{rr}^f(R_i) = \sigma_{rr}^h(R_i)$ and the stress-free condition on the external surface $\sigma_{rr}^h(R_e) = 0$ provide two additional equations. Then the equality of axial displacements $u_z^f = u_z^h$ allows us to write $K^f = K^h = K$, where $K$ is here unknown. In order to solve this problem, we need an additional equation which is given by the global force balance of the cylinder:

$$\int_0^{R_i} r\sigma_z^f \, dr + \int_{R_i}^{R_e} r\sigma_z^h \, dr = 0. \tag{16}$$

Using the geometry and the mechanical characteristics given in table 1, we obtain $C^f = \varepsilon_r^f = 1820 \ \mu\epsilon$, $D^h \approx 0$. Thus $C^h = -11\,400 \ \mu\epsilon \approx \varepsilon_r^h$ and $K = \varepsilon_z = -11\,400 \ \mu\epsilon$.

The cylinder contraction due to the thermal expansion leads to axial compression of the FBG. Because of the effect of Poisson's ratio, the FBG radius increases while the host structure contracts radially.

According to relation (5) expanded with the term relating to the thermal change (see (17)), we calculate the shift in Bragg wavelength caused by a drop of 100 K in temperature:

$$\frac{\Delta\lambda_B}{\lambda_B} = -\frac{n_{\text{eff}}^2}{2}(p_{11} + p_{12})\varepsilon_r + \left(1 - \frac{n_{\text{eff}}^2}{2}p_{12}\right)\varepsilon_z + a\Delta T \tag{17}$$

where $a \approx 7.8 \times 10^{-6}$ K$^{-1}$. If we suppose that the initial Bragg wavelength is 1550 nm, then the shift in wavelength is valued at $-15.29$ nm.

The analysis of the wavelength shift according to equation (6) and the additional term $a\Delta T$ provide an axial strain $\varepsilon_z$ of $-11\,234$ $\mu\epsilon$, which gives a relative error of 1.45% with the real strain of $-11\,400$ $\mu\epsilon$.

*2.3.2. Case study 2: the cylinder external surface is free to move radially while the upper and lower sections are fixed*
In this second thermal load analysis, we choose to fix the axial strain to 0: $\varepsilon_z = 0$. Therefore, the cylinder undergoes deformation only radially. This problem can be solved by using the same equations as in the previous example.

The drop of 100 K in temperature causes a radial strain $\varepsilon_r^{\mathrm{h}} = -15\,960$ $\mu\epsilon$ in the resin and $\varepsilon_r^{\mathrm{f}} = -397$ $\mu\epsilon$ in the FBG, and therefore a shift in Bragg wavelength of $-0.974$ nm. The analysis of these data using relation (6) leads us to conclude that the FBG undergoes an axial extension of 188 $\mu\epsilon$ while it actually undergoes a purely radial strain.

Of course, the two previous case studies are purely academic. The real difficulty in the analysis of optical signals for applications in production process monitoring is that the boundary conditions are very seldom well known. So the real boundary conditions would not probably be the same as in either of the two cases studied here, which shows that it would be difficult to accurately analyze the shift in wavelength using the usual equations.

*2.4. Conclusion about the shift in Bragg wavelength analysis in response to a mechanical load*

These few examples show the necessity of considering a model of coupled strains between the FBG and the host material in order to measure the strain in the case of embedded sensors. According to equation (5) the resolution of such a problem requires us to find two unknown quantities even for an isotropic material. Then, it is essential to make two measurements, which is not possible using classical FBG sensors and their associated interrogation devices. Does this mean that the employment of the FBG strain sensor has to be restricted to surface measurement? We do not think so.

On the contrary, the point of this paper is to show that it is possible to design sensor architecture with only one fiber. Moreover, these structures have to be based only on a measurement of the shift in wavelength, in order to keep the simplicity of the current sensor interrogation methods, allowing us to perform *in situ* monitoring measurement.

In the rest of the paper, several new architectures of sensors are proposed and their performance studied. We show that it is possible to design efficient structures for *in situ* strain measurement by using embedded sensors.

## 3. How to measure $\varepsilon_z$ and $\varepsilon_r$ simultaneously?

Two linearly independent quantities have to be measured to determine axial and radial strains. Several architectures can perform this task. We focus on the following ones: two superimposed FBGs with very different periods; one FBG written inside a birefringent fiber; an FBG and an LPG juxtaposed.

The former architectures can be described by the same formalism, since both correspond to the propagation of core modes. However, we shall study them separately for the sake of clarity. We shall first describe an architecture with two FBGs of very different periods and analyze its efficiency, in order to determine the critical parameters. We shall then apply this analysis to the birefringent sensor. In a second part, we shall study the configuration with a short and a long period grating. The analysis is very different in this case since one mode propagates in the core whereas the others propagate in the cladding. We shall see that this architecture leads to a far better sensitivity.

*3.1. Two FBGs with very different periods*

In this structure, two FBGs with very different periods, $\Lambda_1$ and $\Lambda_2$, are written simultaneously like Moiré gratings. Obviously, their respective Bragg wavelengths $\lambda_1$ and $\lambda_2$ also differ significantly. So, when this sensor is illuminated by a broadband light, it reflects two narrow peaks centered on $\lambda_1$ and $\lambda_2$.

The effective index of the core mode varies with wavelength because of the dispersion. The effective index for the Bragg wavelength $\lambda_1$ is $n_1 = n_{\mathrm{eff}}(\lambda_1)$, and $n_2 = n_{\mathrm{eff}}(\lambda_2) = n_1 + B$ for the Bragg wavelength $\lambda_2$. $B$ increases with the difference between $\lambda_2$ and $\lambda_1$. For example, if the gratings are written in an SMF28 fiber, then $B = 1 \times 10^{-3}$ for $\lambda_1 = 1300$ nm and $\lambda_2 = 1550$ nm.

Let us call $\lambda_{10}$ and $\lambda_{20}$ the Bragg wavelengths when the sensor is free: $\lambda_{10} = 2n_1\Lambda_1$ and $\lambda_{20} = 2n_2\Lambda_2$. When a load is applied, the shifts in Bragg wavelength according to (4) are

$$\begin{aligned} \delta\lambda_1 = \lambda_1 - \lambda_{10} = a_{1z}\varepsilon_z + a_{1r}\varepsilon_r \\ \delta\lambda_2 = \lambda_2 - \lambda_{20} = a_{2z}\varepsilon_z + a_{2r}\varepsilon_r \end{aligned} \quad (18)$$

where

$$\begin{aligned} a_{iz} &= \left(1 - \frac{n_i^2}{2}p_{12}\right)\lambda_i \\ a_{ir} &= -\frac{n_i^2}{2}(p_{11} + p_{12})\lambda_i \end{aligned} \quad i = \{1, 2\}. \quad (19)$$

This system has a unique solution only if

$$D = a_{1z}a_{2r} - a_{1r}a_{2z} \neq 0. \quad (20)$$

Here, $B$ is very small:

$$\begin{aligned} a_{2z} &\simeq a_{1r}\left(1 + \frac{3B}{\Lambda_1^2}\right)\frac{\Lambda_1}{\Lambda_2} \\ a_{2r} &\simeq a_{1z}\left(1 + \frac{B}{n_1}\frac{1 - \frac{3}{2}n_1^2p_{12}}{1 - \frac{1}{2}n_1^2p_{12}}\right)\frac{\Lambda_1}{\Lambda_2}. \end{aligned} \quad (21)$$

These relations imply that $a_{2r} - a_{1r}$ is of the order of $B$ and $a_{2z} - a_{1z}$ is of the order of $B/10$. Finally, $D$ is of the order of

$B$ as well. It is small but different from zero. The system (18) can then be solved:

$$\varepsilon_z = \frac{a_{2r}\,\delta\lambda_1 - a_{1r}\,\delta\lambda_2}{D}$$
$$\varepsilon_r = \frac{a_{1z}\,\delta\lambda_2 - a_{2z}\,\delta\lambda_1}{D}. \tag{22}$$

The uncertainty on $\varepsilon_z$ and $\varepsilon_r$ is calculated from (22):

$$\Delta\varepsilon_z = \frac{|a_{1r}| + |a_{2r}|}{|D|}\,\delta\lambda_{\min}$$
$$\Delta\varepsilon_r = \frac{|a_{1z}| + |a_{2z}|}{|D|}\,\delta\lambda_{\min} \tag{23}$$

where $\delta\lambda_{\min}$ is the smallest detectable shift. It is approximately 1 pm when measured with the best devices.

If we consider again the configuration where $B = 1 \times 10^{-3}$ ($\lambda_1 = 1300$ nm and $\lambda_2 = 1550$ nm) and $\delta\lambda_{\min} = 1$ pm, then $\Delta\varepsilon_z = 1000~\mu\varepsilon$ and $\Delta\varepsilon_r = 1700~\mu\varepsilon$, which is not acceptable. This architecture cannot be used. As a matter of fact, $\Delta\varepsilon$ is conversely proportional to $D$, and then to $B$. In order to reduce $\Delta\varepsilon$ it is necessary to increase $B$. This is hard to do with gratings of different periods but may be tried with birefringent fibers.

### 3.2. One FBG in a birefringent fiber

When an FBG is written inside a birefringent fiber with eigen-axes $\vec{e}_x$ and $\vec{e}_y$, it can be decomposed into two gratings. The waves linearly polarized in the $\vec{e}_x$ direction meet with a grating with effective index $n_1 = n_{\text{eff}x}$, whereas the waves linearly polarized in the $\vec{e}_y$ direction meet with a grating with effective index $n_2 = n_{\text{eff}y} = n_{\text{eff}x} + B$. The Bragg wavelengths associated with each grating are given by relation (1). When the incoming wave is not linearly polarized in the $\vec{e}_x$ or the $\vec{e}_y$ direction, the reflected spectrum is made of two peaks centered on the Bragg wavelengths. However, in this case the two gratings have the same period, and the two peaks are then very close. For classical gratings with a bandwidth of several hundred picometers, $B$ must be greater than $1 \times 10^{-4}$ so that the two peaks are distinguishable.

The most birefringent fibers commercially available have a birefringence of $3 \times 10^{-4}$. Higher birefringence can be reached with special fibers. For example, a birefringence of $1.5 \times 10^{-2} - 4 \times 10^{-2}$ has been experimentally obtained with silica microfibers [13, 14]. Microstructured fibers could also lead to a very high birefringence: simulations [15, 16] have shown that fibers with elliptical holes could have a birefringence of $1 \times 10^{-2} - 5 \times 10^{-2}$.

Under optimal conditions $B = 5 \times 10^{-2}$ and $\delta\lambda_{\min} = 1$ pm. According to (23), the uncertainties are then $\Delta\varepsilon_z = 20~\mu\varepsilon$ and $\Delta\varepsilon_r = 30~\mu\varepsilon$. Moreover, the measure can be analyzed only if $\delta\lambda_1$ and $\delta\lambda_2$ are greater than $\delta\lambda_{\min}$. In the strain space $(\varepsilon_z, \varepsilon_r)$, this condition holds outside an area inscribed in a rectangle of dimensions $40~\mu\varepsilon \times 60~\mu\varepsilon$ (cf figure 4). We can then consider that the accuracy of the measurement is in this case approximately $30~\mu\varepsilon$.

Finally, this architecture is characterized by poor performance although it requires high technology fibers. It is therefore not relevant.
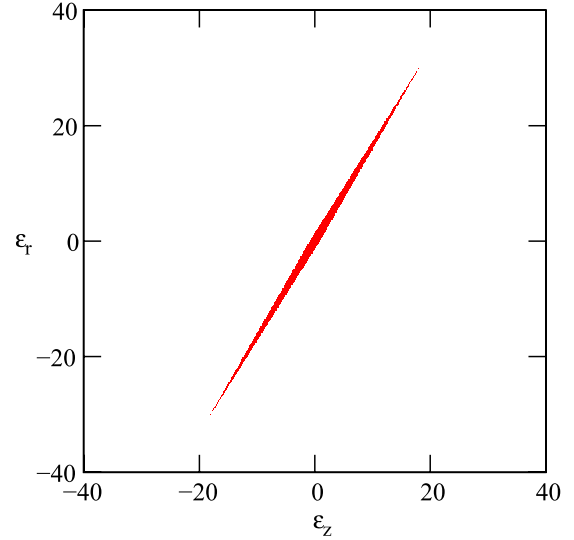


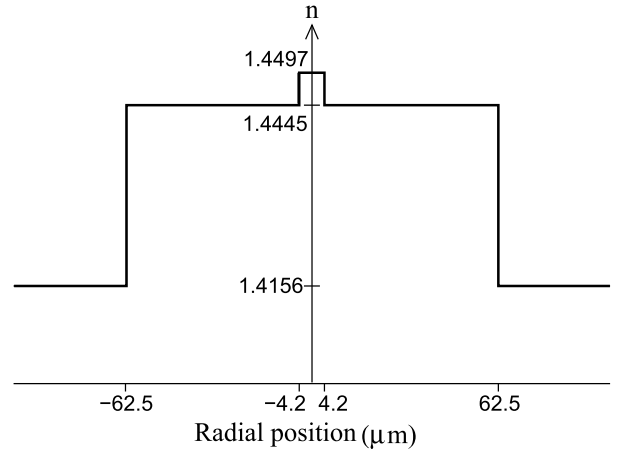**Figure 4.** Inside the colored zone, the Bragg wavelength shifts are smaller than 1 pm.



**Figure 5.** Radial index profile for the wavelength $\lambda = 1540$ nm.

### 3.3. A short and a long period grating

*3.3.1. Description of the sensor.* In this structure, a short period grating is juxtaposed with a long period grating. Under the conditions where equation (6) holds, this structure is known to be able to measure simultaneously strain and temperature accurately [4, 5]. We shall now see if it can also discriminate axial and radial strain.

We consider a three-layer optical fiber. Such a fiber has already been experimentally tried (see for example [17]). The inner core layer is surrounded by two cladding layers. All the layers are made of quenched glass with slightly different doping. Their mechanical properties are then the same, but their refractive index decreases by steps from the center (see figure 5).

The short period grating reflects a narrow spectral band of the incoming light centered on the Bragg wavelength: $\lambda_{\text{FBG}} = n_{\text{FBG}}\Lambda_{\text{FBG}}$, where $n_{\text{FBG}}$ is the effective index of the core mode at $\lambda_{\text{FBG}}$ and $\Lambda_{\text{FBG}}$ the period of the grating. As a consequence, the transmitted spectrum exhibits a hole centered at $\lambda_{\text{FBG}}$.

6

Inside the long period, there is a coupling between the core mode and several resonant cladding modes. This means that, for resonant wavelengths, the light is transferred from the core to the cladding, where it vanishes because of losses. The transmitted spectrum also shows several holes around these resonant wavelengths. The resonance condition is

$$\lambda_{\mathrm{LPG}} = (n_{\mathrm{eff}} - n_{\mathrm{LPG}})\Lambda_{\mathrm{LPG}} \tag{24}$$

where $n_{\mathrm{eff}}$ is the effective index of the core mode at $\lambda_{\mathrm{LPG}}$, $n_{\mathrm{LPG}}$ is the effective index of the cladding mode at $\lambda_{\mathrm{LPG}}$ and $\Lambda_{\mathrm{LPG}}$ the period of the grating. We assume that the outer cladding is large enough to be considered as semi-infinite. The effective index of the cladding mode is then given by the dispersion equation [18]:

$$\begin{aligned}
&\zeta_0(\lambda, a_1, a_2, n_1, n_2, n_3, n_{\mathrm{LPG}}) \\
&= \zeta_0'(\lambda, a_1, a_2, n_1, n_2, n_3, n_{\mathrm{LPG}})
\end{aligned} \tag{25}$$

where $a_1$ is the core radius, $a_2$ the inner cladding radius, $n_1$ the core refractive index, $n_2$ the inner cladding refractive index and $n_3$ the outer cladding refractive index. The functions $\zeta_0$ and $\zeta_0'$ are detailed in the appendix.

When the fiber is strained, $n_1$, $n_2$ and $n_3$ vary according to (4) and $a_1$ and $a_2$ vary as

$$a_{\mathrm{i}} = (1 + \varepsilon_r)a_{i0} \tag{26}$$

where $a_{i0}$ are the radii in the unstrained configuration. However, the variation of the effective index of the cladding modes does not obey law (4). It is then not possible to write explicit equations that link the variation of the resonant wavelengths to the coefficients of the photo-elastic tensor, as we have done for the FBG. In this case, the dispersion equation (25) should be solved numerically to determine the response of the LPG to strain.

*3.3.2. Sensitivity analysis.* The following parameters have been used to perform the simulations: $a_{10} = 4.2 \ \mu$m and $a_{20} = 62.5 \ \mu$m; $\Lambda_{\mathrm{FBG}} = 535.7$ nm and $\Lambda_{\mathrm{LPG}} = 48.16 \ \mu$m. The resonant wavelengths in the unstrained configuration are 1550 nm for the short period grating and 1540 nm for the long period grating. Since the dispersion equations depend on the wavelength, it is necessary to take into account the variation of the refractive index with the wavelength. In the transparency regions, these variations are described by a Sellmeier law:

$$n^2(\lambda) = 1 + \sum_{j=1}^{N} \frac{A_j \lambda^2}{\lambda^2 - \lambda_j^2}$$

where $A_j$, $\lambda_j$ and $N$ depend on the material. For the inner cladding, we use the coefficients given by Bhatia [19] for quenched glass: $A_1 = 0.696\,750$, $A_2 = 0.408\,218$, $A_3 = 0.890\,815$, $\lambda_1 = 0.069\,066 \ \mu$m, $\lambda_2 = 0.115\,662 \ \mu$m and $\lambda_3 = 9.900\,559 \ \mu$m. For the refractive index of the core and the outer cladding, we follow Lundin's approach [20, 21] and assume that $n_{1,3}(\lambda) = N_{1,3} \ n_2(\lambda)$, where $N_1 = 1.0036$ and $N_3 = 0.98$ do not depend on wavelength.

In order to determine the shift of $\lambda_{\mathrm{LPG}}$ due to strain, the variation of $n_1$, $n_2$ and $n_3$ is computed for each $(\varepsilon_r, \varepsilon_z)$ according to (4) and the variation of $a_1$ and $a_2$ according
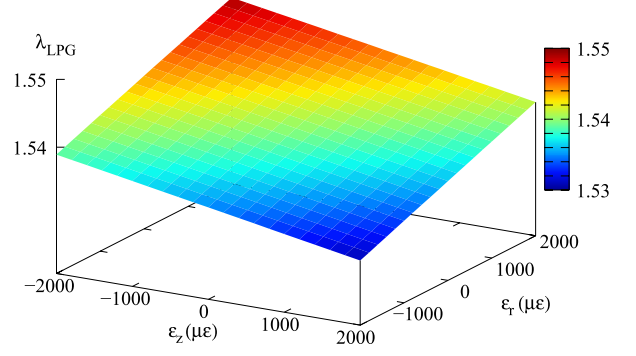


**Figure 6.** Evolution of $\lambda_{\mathrm{LPG}}$ as a function of $(\varepsilon_z, \varepsilon_r)$.
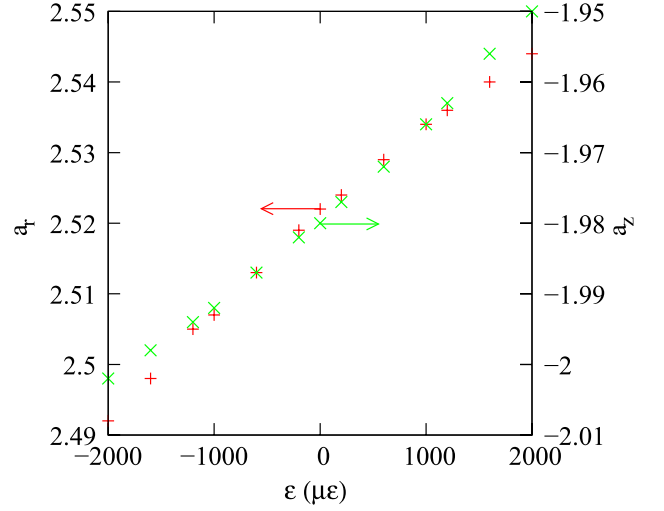


**Figure 7.** Evolution of $a_{2z}$ ($a_{2r}$) as a function of $\varepsilon_r$ ($\varepsilon_z$).

to (26). Then we solve numerically (24) by using a simple bisection algorithm. Figure 6 shows the variation of $\lambda_{\mathrm{LPG}}$ as a function of the radial and axial strains, in the range $\pm 2000 \ \mu\varepsilon$. At first glance, this variation is linear in $\varepsilon_z$ and $\varepsilon_r$:

$$\lambda_{\mathrm{LPG}} = a_{2z} \ \varepsilon_z + a_{2r} \ \varepsilon_r + \lambda_{\mathrm{LPG}0}. \tag{27}$$

However, a more careful examination of these results shows that the factor of proportionality ($a_{2z}$ or $a_{2r}$) between the resonant wavelength and the strain in one direction depends on the strain in the other direction. This appears clearly in figure 7: $a_{2z}$ and $a_{2r}$ have a variation of 1% in the considered range of strain. This is the limit of the linear approximation (27).

A linear fit of the calculated $\lambda_{\mathrm{LPG}}$ according to (27) gives the coefficients $a_{2z} = -1.98$ pm/$\mu\varepsilon$ and $a_{2r} = 2.52$ pm/$\mu\varepsilon$. The parameters of the short period grating are the same as in the previous section: $a_{1z} = 1.12$ pm/$\mu\varepsilon$ and $a_{1r} = -0.57$ pm/$\mu\varepsilon$. We can write with these coefficients a system similar to (18). In this case $|D| = 1.49/\mu\varepsilon^2$. This value is much greater than those in the other configurations. We then expect a far better efficiency. Indeed, in the $(\varepsilon_z, \varepsilon_z)$ plane, the region where $\delta\lambda_1$ and $\delta\lambda_2$ are greater than $\delta\lambda_{\min} = 1$ pm lies outside a parallelogram inscribed in a $3 \ \mu\varepsilon \times 3 \ \mu\varepsilon$ area (cf figure 8). Moreover, according to (23), the uncertainties
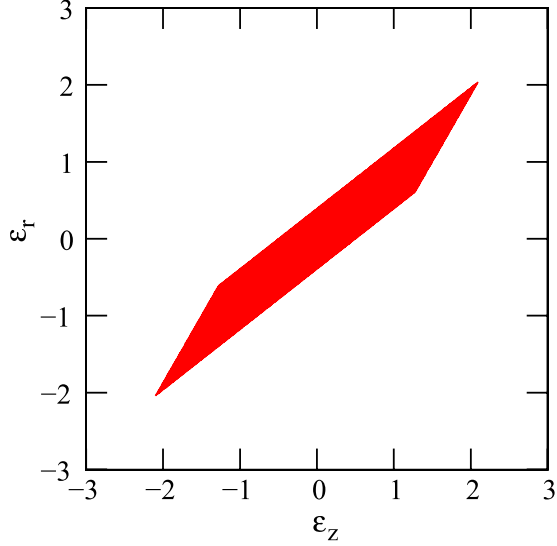
**Figure 8.** In the colored area, the shifts in resonant wavelengths are smaller than 1 pm for both gratings.

on the measured strains are in this case $\Delta\varepsilon_z \approx \Delta\varepsilon_r \approx 2\ \mu\varepsilon$. Therefore, this sensor is able to measure simultaneously $\varepsilon_z$ and $\varepsilon_r$ with the same accuracy as classical FBG sensors.

Before concluding, let us discuss the possibility of manufacturing the proposed structure by focusing on three questions: is it possible to make a three-layer fiber? Can we obtain refractive index differences such as those used in the sensitivity analysis? Is it possible to inscribe an LPG and an FBG together inside the core of the fiber?

The answer to all these questions is definitely yes. In the classical manufacturing methods, the preform is made by vapor deposition on or inside a rotating tube. Such a method is perfectly adapted to the production of multiple concentric layers [22]. Indeed, several fibers of this kind are already commercially available (see for example W fibers or double-core fibers used in fiber lasers).

The second issue relates to the refractive index difference between the three layers. It is the same between the core and the inner cladding as in a standard SMF28 fiber. It is about 0.03 between the inner and the outer cladding. This value corresponds to a difference in the concentration in $GeO_2$ of approximately 20 mol.%. Such a concentration can be easily obtained [23] since higher differences have already been achieved [24].

Finally, the problem of the juxtaposition of an FBG and an LPG should be addressed. Such a structure has already been made by several research teams [4, 5], with classical inscription methods. Their experimental fabrication protocol could then be easily applied to industry. As a conclusion, the proposed sensor, though not currently existent, can be manufactured with available tools and techniques.

## 4. Conclusion

Most of the time, when an FBG is used as a strain sensor, the linear relation between the radial and axial strains $\varepsilon_r =$ $-\nu\varepsilon_z$ is implicitly assumed. With this assumption, only one unknown is left and the measurement of the Bragg wavelength shift is enough to characterize the whole strain. This perfectly holds when the FBG is glued on two points on the surface of the observed structure. This is not true any more when the FBG is embedded in a host material. In this paper we studied this configuration, with different mechanical and thermal loads. We then showed that it was sometimes absolutely necessary to determine both axial and radial strains so as to avoid erroneous measurements of the axial strain.

We then proposed several kinds of sensor able to measure simultaneously $\varepsilon_r$ and $\varepsilon_z$. The first ones were based on two core modes with different effective indices. The analysis of sensitivity showed that this kind of structure can hardly discriminate the axial and radial strain. They could be used if the difference of effective indices between the two modes was higher than $1 \times 10^{-1}$. This does not seem feasible with classical fibers, but could be realized with photonic crystal fiber.

The most promising structure is made of the juxtaposition of a short period grating and a long period grating. This configuration uses a core mode and a cladding mode which have very different sensitivities to axial and radial strains. This is a key point for an efficient discrimination of the two strains. Indeed, we showed that it was possible to reach an accuracy of the order of $2\ \mu\varepsilon$ on both strains. In other words, this sensor is as accurate as classical FBG sensors, but it keeps its accuracy and reliability when embedded in a host material, while the strain remains uniform along the grating and isotropic in the transverse plane.

## Appendix. Dispersion equation of the cladding modes

$$\zeta_0 = \frac{1}{\sigma_2}\left\{ u_2\left(JK + \frac{\sigma_1\sigma_2 u_{21} u_{32}}{n_2^2 a_1 a_2}\right)p_1(a_2) - Kq_1(a_2)\right.$$
$$+ Jr_1(a_2) - \frac{1}{u2}s_1(a_2)\right\}\left\{-u_2\left(\frac{u_{32}}{n_2^2 a_2}J - \frac{u_{21}}{n_1^2 a_1}K\right)\right.$$
$$\left. + \frac{u_{32}}{n_1^2 a_2}q_1(a_2) + \frac{u_{21}}{n_1^1 a_1}r_1(a_2)\right\}^{-1} \tag{A.1}$$

and

$$\zeta_0' = \sigma_1\left\{u_2\left(\frac{u_{32}}{a_2}J - \frac{n_3^2 u_{21}}{n_2^2 a_1}K\right)p_1(a_2) - \frac{u_{32}}{a_2}q_1(a_2)\right.$$
$$\left. - \frac{u_{21}}{a_1}r_1(a_2)\right\}\left\{u_2\left(\frac{n_3^2}{n_2^2}JK + \frac{\sigma_1\sigma_2 u_{21} u_{32}}{n_1^2 a_1 a_2}\right)p_1(a_2)\right.$$
$$\left. - \frac{n_3^2}{n_1^2}Kq_1(a_2) + Jr_1(a_2) - \frac{n_2^2}{n_1^2 u_2}s_1(a_2)\right\}^{-1} \tag{A.2}$$

with

$$\sigma_1 = in_{\text{LPG}}/Z_0 \qquad (A.3)$$

$$\sigma_2 = in_{\text{LPG}}Z_0 \qquad (A.4)$$

where $Z_0 = 377 \ \Omega$ is the electromagnetic impedance in vacuum

$$u_{21} = \frac{1}{u_2^2} - \frac{1}{u_1^2} \qquad (A.5)$$

$$u_{32} = \frac{1}{w_3^2} + \frac{1}{u_2^2} \qquad (A.6)$$

knowing that

$$u_j^2 = (2\pi/\lambda)^2(n_j^2 - n_{\text{LPG}}^2) \qquad (A.7)$$

$$w_3^2 = (2\pi/\lambda)^2(n_{\text{LPG}}^2 - n_3^2) \qquad (A.8)$$

and

$$J = \frac{J_1'(u_1 a_1)}{u_1 J_1(u_1 a_1)} \qquad (A.9)$$

$$K = \frac{K_1'(w_3 a_2)}{w_3 K_1(w_3 a_2)} \qquad (A.10)$$

$$p1(r) = J1(u_2 r)N_1(u_2 a_1) - J_1(u_2 a_1)N_1(u_2 r) \quad (A.11)$$

$$q1(r) = J1(u_2 r)N_1'(u_2 a_1) - J_1'(u_2 a_1)N_1(u_2 r) \quad (A.12)$$

$$r1(r) = J'1(u_2 r)N_1(u_2 a_1) - J_1(u_2 a_1)N_1'(u_2 r) \quad (A.13)$$

$$s1(r) = J'1(u_2 r)N_1'(u_2 a_1) - J_1'(u_2 a_1)N_1'(u_2 r). \quad (A.14)$$

$J$ is a Bessel function of the first kind, $K$ a modified Bessel function of the second kind and $N$ a Bessel function of the second kind. The prime sign denotes the derivation with respect to the total argument.

# References

[1] Kang H K, Kang D H, Bang H J, Hong C S and Kim C G 2002 Cure monitoring of composite laminates using fiber optic sensors *Smart Mater. Struct.* **11** 279

[2] Leng J S and Asundi A 2002 Real-time cure monitoring of smart composite materials using extrinsic Fabry–Perot interferometer and fiber Bragg grating sensors *Smart Mater. Struct.* **11** 249–55

[3] Xu M G, Archambault J L, Reekie L and Dakin J P 1994 Discrimination between strain and temperature effects using dual-wavelength fibre grating sensors *Electron. Lett.* **30** 1085–7

[4] Chi H, Tao X-M, Yang D-X and Chen K-S 2001 Simultaneous measurement of axial strain, temperature, and transverse load by a superstructure fiber grating *Opt. Lett.* **26** 1949–51

[5] Triollet S, Robert L, Marin E and Ouerdane Y 2011 Discriminated measures of strain and temperature in metallic specimen with embedded superimposed long and short fibre Bragg gratings *Meas. Sci. Technol.* **22** 015202

[6] Hill K O and Meltz G 1997 Fiber Bragg grating technology fundamentals and overview *J. Lightwave Technol.* **15** 1263–76

[7] Gebremichael Y M *et al* 2005 Integration and assessment of fibre bragg grating sensors in an all-fibre reinforced polymer composite road bridge *Sensors Actuators A: Phys.* **118** 78–85

[8] Propst A, Peters K, Zikry M A, Schultz S, Kunzler W, Zhu Z, Wirthlin M and Selfridge R 2010 Assessment of damage in composite laminates through dynamic, full-spectral interrogation of fiber Bragg grating sensors *Smart Mater. Struct.* **19** 015016

[9] Gafsi R and El-Sherif M A 2000 Analysis of induced-birefringence effects on fiber bragg gratings *Opt. Fiber Technol.* **6** 299–323

[10] Timoshenko S and Goodier J N 1969 *Theory of Elasticity* (New York: McGraw-Hill)

[11] Bertholds A and Dandliker R 1988 Determination of the individual strain-optic coefficients in single-mode optical fibers *J. Lightwave Technol.* **6** 17

[12] Khoun L, Oliveira R, Michaud V and Hubert P 2011 Investigation of process-induced strains development by fibre bragg grating sensors in resin transfer moulded composites *Composites* A **42** 274–82

[13] Xuan H, Ju J and Jin W 2010 Highly birefringent optical microfibers *Opt. Express* **18** 3828–39

[14] Kou J, Xu F and Lu Y 2011 Highly birefringent slot-microfiber *IEEE Photon. Technol. Lett.* **23** 1034–6

[15] Yue Yang *et al* 2007 Highly birefringent elliptical-hole photonic crystal fiber with squeezed hexagonal lattice *Opt. Lett.* **32** 469–71

[16] Chau Y F, Liu C Y, Yeh H H and Tsai D P 2010 A comparative study of high birefringence and low confinement loss photonic crystal fiber employing elliptical air holes in fiber cladding with tetragonal lattice *Prog. Electromagnetics Res.* **22** 39–52

[17] Allsop T, Webb D J and Bennion I 2003 A comparison of the sensing characteristics of long period gratings written in three different types of fiber *Opt. Fiber Technol.* **9** 210–23

[18] Erdogan T 1997 Cladding-mode resonances in short- and long-period fiber grating filters *J. Opt. Soc. Am.* A **14** 1760–73

[19] Bhatia V 1996 Properties and sensing applications of long-period gratings *PhD Thesis* Virginia Tech. Blackburg

[20] Lundin R 1993 Minimization of the chromatic dispersion over a broad wavelength range in a single-mode optical fiber *Appl. Opt.* **32** 3241–5

[21] Lundin R 1994 Dispersion flattening in a W fiber *Appl. Opt.* **33** 1011–4

[22] Kehrli M, Tosin P, Luthy W and Weber H P 2000 Manufacture of fibres with multiple claddings *Laser Phys.* **10** 458–60

[23] Fleming J W and Wood D L 1983 Refractive index dispersion and related properties in fluorine doped silica *Appl. Opt.* **22** 3102–4

[24] Mashinsky V M *et al* 2004 Germania-glass-core silica-glass-cladding modified chemical-vapor deposition optical fibers: optical losses, photorefractivity, and Raman amplification *Optics Lett.* **29** 2596–8